

Aging-Aware Training for Printed Neuromorphic Circuits

Haibin Zhao

haibin.zhao@kit.edu

Karlsruhe Institute of Technology

Karlsruhe, Germany

Michael Beigl

michael.beigl@kit.edu

Karlsruhe Institute of Technology

Karlsruhe, Germany

Michael Hefenbrock

michael.hefenbrock@kit.edu

Karlsruhe Institute of Technology

Karlsruhe, Germany

Mehdi B. Tahoori

mehdi.tahoori@kit.edu

Karlsruhe Institute of Technology

Karlsruhe, Germany

ABSTRACT

Printed electronics allow for ultra-low-cost circuit fabrication with unique properties such as flexibility, non-toxicity, and stretchability. Because of these advanced properties, there is a growing interest in adapting printed electronics for emerging areas such as fast-moving consumer goods and wearable technologies. In such domains, analog signal processing in or near the sensor is favorable. Printed neuromorphic circuits have been recently proposed as a solution to perform such analog processing natively. Additionally, their learning-based design process allows high efficiency of their optimization and enables them to mitigate the high process variations associated with low-cost printed processes. In this work, we address the aging problem of the printed components. This effect can significantly degrade the accuracy of printed neuromorphic circuits over time. For this, we develop a stochastic aging-model to describe the behavior of aged printed resistors and modify the training objective by considering the expected loss over the lifetime of the device. This approach ensures to provide acceptable accuracy over the device lifetime. Our experiments show that an overall 35.8% improvement in terms of expected accuracy over the device lifetime can be achieved using the proposed learning approach.

CCS CONCEPTS

- Hardware → Aging of circuits and systems; Neural systems;
- Computing methodologies → Machine learning approaches.

KEYWORDS

printed electronics, neuromorphic computing, aging model, aging-aware training

ACM Reference Format:

Haibin Zhao, Michael Hefenbrock, Michael Beigl, and Mehdi B. Tahoori. 2022. Aging-Aware Training for Printed Neuromorphic Circuits. In *IEEE/ACM International Conference on Computer-Aided Design (ICCAD '22)*, October 30–November 3, 2022, San Diego, CA, USA. ACM, New York, NY, USA, 9 pages. <https://doi.org/10.1145/3508352.3549411>

Permission to make digital or hard copies of all or part of this work for personal or classroom use is granted without fee provided that copies are not made or distributed for profit or commercial advantage and that copies bear this notice and the full citation on the first page. Copyrights for components of this work owned by others than the author(s) must be honored. Abstracting with credit is permitted. To copy otherwise, or republish, to post on servers or to redistribute to lists, requires prior specific permission and/or a fee. Request permissions from permissions@acm.org.

ICCAD '22, October 30–November 3, 2022, San Diego, CA, USA

© 2022 Copyright held by the owner/author(s). Publication rights licensed to ACM.

ACM ISBN 978-1-4503-9217-4/22/10...\$15.00

<https://doi.org/10.1145/3508352.3549411>

1 INTRODUCTION

With novel products such as wearable medical devices and Internet of Things (IoT) infrastructures stepping into our daily lives, stretchable, non-toxic, flexible, and low-cost electronics become desperately requested [32, 43]. Classic, conventionally fabricated silicon-based circuitry cannot meet these requirements. Consequently, printed electronics (PE) dominates the emerging areas for meeting these demands [47]. Additionally, on-demand on-site fabrication and much-reduced fabrication costs over classical silicon technologies make PE particularly promising for such domains.

Several printing methods exist, such as jet-printing [15], screen-printing [29] or gravure printing [22]. Among the emerging printing technologies, inkjet-printing [28, 53] is a promising candidate as it enables low-cost on-demand and on-site fabrication as well as low-voltage operation [10] to be integrated with printed energy harvesters [33, 37].

In practice, most sensors convert information into electrical signals and transmit them to analog-digital converters (ADC). From there, signals are transmitted to digital computing devices, such as micro-controllers or even the cloud, for further analysis. However, some simple tasks such as stress detection [8] and air quality monitoring [59] could be solved without an ADC, signal transmission, or extensive computing resources. One of the most promising approaches to fulfill these requirements is the printed neuromorphic circuits [56]. Here, signal processing is done directly on analog data without the need for costly ADC. Neuromorphic circuits are composed of multiple printed neurons connected by printed wires. Each neuron consists of a crossbar implementing a weighted-sum and a circuit realizing a non-linear transformation. The latter serves as the activation function in artificial neural networks. See Section 2 for more details.

Due to the limitation of the low-cost additive printing technology, the conductive properties of actually printed devices will inevitably deviate from the intended design values. Furthermore, due to environmental influences and particularly thermal stress in the field, the thin-film printed devices exhibit run-time degradation through usage (*aging*) [6, 26, 38]. As a result, the conductances of printed resistors such as Indium Tin Oxide (ITO) will change over time [27]. These effects lead to deviations from the intended design values of weights in the neuromorphic circuit over time and may ultimately result in misclassifications.

To address the aging problem in printed neuromorphic circuits, we propose an approach to increase the robustness against aging

via a modified training objective based on aging models of the circuit components. Through the modified objective, aging effects can be anticipated in training, and, instead of only considering the initial circuit (non-aged) accuracy, the accuracy over the device lifetime is considered and optimized during training. In summary, the contributions of this work are:

- We develop a variation model for the aging of printed resistors.
- We reduce the number of hyperparameters of printed neural network (pNN) training by use of the straight-through estimator.
- We propose an aging-aware training solution for pNN to address the aging problem of printed neuromorphic circuits.

While the methods proposed in this work are evaluated for printed technologies, the overall methodology may also help in addressing aging effects in other technologies.

The rest of this work is structured as follows: To aid the understanding of the material presented, Section 2 briefly introduces printed electronics and printed neural networks. Section 3 describes the aging model as well as the aging-aware training of the pNN, while Section 4 gives the evaluation of our proposed algorithm. Finally, Section 5 concludes this paper and discusses possible directions for future work.

2 PRELIMINARIES

As a preliminary, we briefly review the necessary background knowledge regarding PE, printed neuromorphic circuits, and their training.

2.1 Printed Electronics

PE refers to a fabrication technology that is based on various printing processes, such as jet-printing, screen- or gravure-printing [20]. Due to the simple manufacturing process as well as low equipment costs, ultra-low-cost electronic circuits can be fabricated at a drastically lower cost compared to silicon-based VLSI processes, which require expensive foundries and clean rooms, even with older technology nodes.

Rather than replacing silicon-based electronics, PE serves as a complement as it cannot rival silicon-based electronics in terms of performance, integration density, and area. However, PE has several advantages: it is possible to print on several rigid or flexible substrates, such as plastic foil or paper, and enables low-cost production [17, 45].

Printing technologies are broadly divided into two categories. Some printing technologies are based on the purely additive manufacturing process, while others employ subtractive processes as well [12], as shown in Figure 1. In the subtractive process, a series of additive (deposition) and subtractive (etching) steps are involved, similar to silicon-based processing. The subtractive process is relatively expensive compared to the additive process, as it involves highly specialized processing, expensive equipment, and infrastructure. On the other hand, only deposition steps are involved in the additive manufacturing process. Transistors, passive components, and interconnects are realized by depositing material layer-by-layer. Generally, fully-additive printed electronics are slower, have larger feature sizes and suffer from higher variations compared

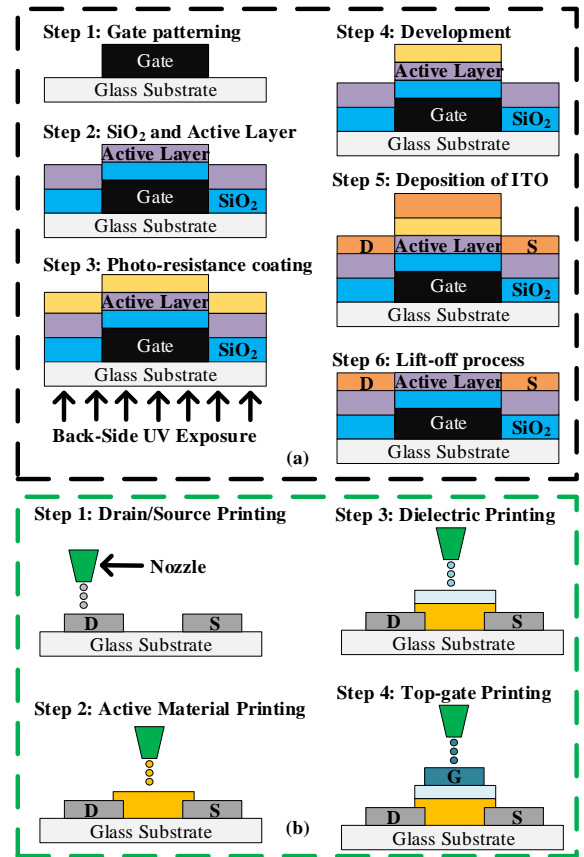


Figure 1: (a) Subtractive based printing process; (b) Fully-additive inkjet printed process.

to the subtractive-based printed technologies. However, the main benefit is much reduced fabrication costs compared to subtractive processes, making them a suitable candidate for ultra-low-cost domains.

Electronics on flexible substrates are enabled by using contactless printing methods. For example, inkjet-printers, in combination with highly optimized functional inks such as conductive, semi-conductive, and non-conductive materials. From these inks, organic [16] or oxide-based [48] transistors can be built. While organic materials are easy to be processed, they have lower environmental stability. On the other side, oxide-based inks have excellent conductivity and environmental stability but are harder to be printed and suffer from impurities due to surfactants [20].

Inkjet-printed electrolyte-gated transistor (EGT) technology is an oxide-based inorganic printed technology that deploys fluid electrolytes as a dielectric substitute in the transistor and allows operating voltages in the sub-1V regime, making it a suitable candidate for self-powered, portable computing systems in the IoT domain.

Despite these promising features, several limitations are prevalent in PE. For example, the large feature sizes and high parasitic capacitances, which lead to low functional densities and high device

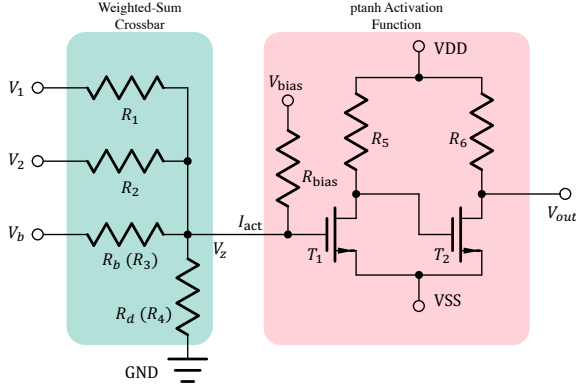


Figure 2: Hardware implementation for a printed neuron. The green part shows the crossbar for weighted-sum and the pink part represents the printed tanh-like non-linear transformation as an activation function.

latencies. Due to this, low-complex circuit designs with limited transistor count are favored to reduce area utilization and to make the designs manufacturable with reasonable yield. Following this trend, several fundamental components for computing systems have already been successfully realized, such as boolean logic [19], digital and analog storage elements [28, 54], or amplifiers [36]. Besides, printed circuits generally exhibit high variations in production [13]. To overcome this drawback, variation could be considered during the design [46].

2.2 Printed neuromorphic circuits

Printed neuromorphic circuits are circuits that use hardware primitives inspired by the brain or artificial neural networks. Their main hardware primitives are the resistor crossbar for realizing the weighted-sum operation and some non-linear circuitry expressing the activation function. Additionally, to implement a notion of negative weights, negative-weight circuits are used to invert input signals emulating a multiplication by a negative number. The individual components will be introduced in detail in the following:

Crossbar weighted-sum. Figure 2 illustrates the hardware implementation for a printed neuron. The green box on the left shows the crossbar structure implementing a weighted-sum operation. According to Kirchhoff's law [35], the following equation holds:

$$\frac{V_z}{R_4} = \frac{V_1 - V_z}{R_1} + \frac{V_2 - V_z}{R_2} + \frac{V_b - V_z}{R_3} - I_{act}.$$

Here, the voltage V_i indicates the input voltage of the crossbar associating with resistance R_i , V_z denotes the output voltage of the crossbar, and $V_b \equiv 1$ denotes the input voltage at the resistor R_b . Since the impedance of the printed activation function (red part in Figure 2) is much higher than that of the crossbar, the current I_{act} can be neglected [57]. Therefore, after the reformulation for V_z and expressing everything in terms of conductances $G_i = 1/R_i$, we obtain

$$V_z \approx \frac{G_1}{G_{\text{sum}}} V_1 + \frac{G_2}{G_{\text{sum}}} V_2 + \frac{G_3}{G_{\text{sum}}} V_b, \quad (1)$$

where $G_{\text{sum}} = \sum_{i=1}^4 G_i$. Evidently, Equation 1 resembles a weighted-sum operation similar to

$$z = w_1 x_1 + w_2 x_2 + b$$

in a neuron equation of a neural network, where z , w_i , x_i and b correspond to V_z , G_i/G_{sum} , V_i and g_b/G_{sum} in Equation 1.

Negative weights. Unfortunately, the weighted-sum operation from Equation 1 only allows expressing specific combinations of weights. Additionally, as the weights are formed through the conductance values of the crossbar resistors, only positive weights can be realized. To emulate the behavior of negative weights, negative-weight circuits are used to transform the input x to $\text{inv}(x)$ instead [56].

Activation function circuits. The last hardware primitive is the so-called activation function circuit. The main requirement for this circuit is to display a non-linear behavior with respect to its input. Several circuits resembling classical activation function of artificial neural networks have been realized in PE, see [56, 57]. A circuit inspired by the tanh function behavior can be seen on the right in Figure 2. The printed tanh function is modeled by

$$\text{ptanh}(x) = \eta_1 + \eta_2 \cdot \tanh((x - \eta_3) \cdot \eta_4)$$

with $\eta_1 = 0.134$, $\eta_2 = 0.962$, $\eta_3 = 0.183$, and $\eta_4 = 24.10$.

Printed neural networks. To model the behavior of the neuromorphic circuits and learn a parameterization of its components, the pNN was introduced [56]. A pNN models the behavior of a printed neuromorphic circuits and use so-called surrogate conductances θ_i as learnable parameters. A surrogate conductance encodes the value of printed conductance through its absolute value, i.e., $G_i = |\theta_i|$. Additionally, the sign of θ_i encodes whether the corresponding input x should be inverted through $\text{inv}(x)$ (to emulate the behavior of a negative weight). Hence, the weighted sum operation of a neuron is modeled by

$$\sum_i w_i \left(x_i \cdot \mathbb{1}_{\{\theta_i \geq 0\}} + \text{inv}(x_i) \cdot \mathbb{1}_{\{\theta_i < 0\}} \right),$$

where $\mathbb{1}_{\{\cdot\}}$ denotes an indicator function returning 1 if the respective condition is true, else 0 and

$$w_i = \frac{|\theta_i|}{\sum_j |\theta_j|}.$$

For brevity, all surrogate conductances (learnable parameters) of the pNN are collected in the vector θ .

Training printed neural networks. To obtain the values of the surrogate conductances θ_i , a loss function $\mathcal{L}\{\cdot\}$ (details see [56]) is minimized using gradient-based optimization. However, the values of the surrogate conductances have to be constrained to ensure the feasibility of the resulting conductances.

For this, given the range of technologically feasible conductance values $G \in \{0\} \cup [G_{\min}, G_{\max}]$ (0 relates to not printing), $|\theta|$ also has to satisfy those bounds. More specifically, $\theta \in [-G_{\max}, -G_{\min}] \cup \{0\} \cup [G_{\min}, G_{\max}]$.

To guarantee that these constraints hold, [56] used projections to ensure $\theta_i \in [-G_{\max}, G_{\max}]$. Additionally, after training, $\theta \in [-G_{\min}, G_{\min}]$ are set to 0 after training. To reduce the effect of this final projection to 0, a penalty term is used throughout the training

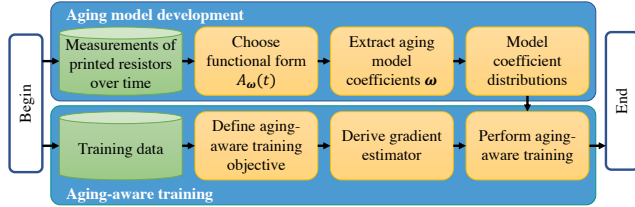


Figure 3: A flowchart of the main steps for aging model development and aging-aware training. The green boxes indicate datasets while the yellow boxes denote steps to be executed.

to avoid $\theta \in [-G_{\min}, G_{\min}]$. Unfortunately, introducing a penalty term requires a weighting coefficient which is a hyperparameter that needs to be tuned.

To avoid this tuning and still make the training algorithm aware of the infeasible region $[-G_{\min}, G_{\min}]$, we directly project the parameters $\theta \in [-G_{\min}, G_{\min}]$ to 0 in the forward pass in training. Usually, this would lead the gradient descent to obtaining a zero-gradient for parameters in the respective regions. However, we can leverage an estimate of the gradient, the so-called straight-through estimator [58], to perform backpropagation through the projection operation. Thus, in the forward pass, we consider

$$\theta_{\text{ste}} = \begin{cases} 0, & |\theta| < G_{\min}, \\ \text{sign}(\theta) \cdot G_{\max}, & |\theta| > G_{\max}, \\ \theta, & \text{otherwise}, \end{cases}$$

while in the backward pass, the gradient of a surrogate conductance θ is considered to be $\nabla_\theta(\theta_{\text{ste}}) = 1$. Through the use of the straight-through estimator and the aforementioned projections, backpropagation can be applied for training and all θ remain feasible throughout the training.

2.3 Related Work

Modeling aging of printed components. Depending on the materials, thin-film printed circuits display considerable run-time degradation over time [6, 11, 26, 38], this is the *aging* effect of printed electronics. Several works have studied the aging effect of resistors to some degree, e.g., the aging of thick-film resistors [18, 50, 51] and the aging of thin-film resistors [3, 9, 27]. A survey of aging effects in both thick and thin film resistors is presented in [39]. However, there is still only few research on the aging of inkjet-printed resistors. For example, although the behavior of printed flexible resistors by thermal, mechanical, and electrical stresses was studied in [7], no relationship between resistance and time was discussed. Hamasha et al. studied the aging of ITO thin film resistors in terms of time under thermal conditions [27], and the result of the experiments shows that the aging of ITO resistance consists mainly of two stages, namely a degradation stage followed by a stable stage. Nevertheless, no mathematical model is given in their work.

Considering aging in neuromorphics. With respect to considering aging effects in the designing of neuromorphic circuits, Zhang et al. proposed a co-optimization framework that combines software and hardware mapping to reduce the aging effect of memristors [7].

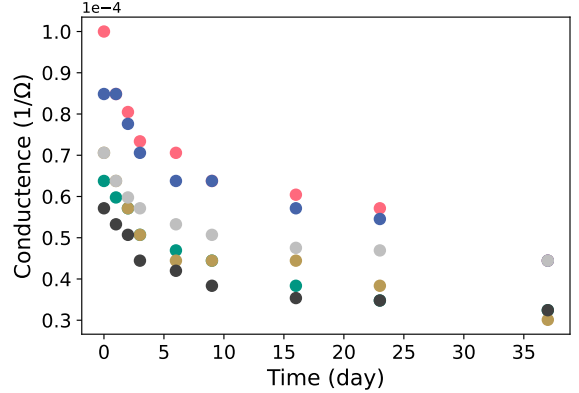


Figure 4: The conductance values of six printed PEDOT resistors measured over 37 days.

Irmanova et al. framed a self-timed programming circuit to address the problem of aging memristors [31]. Although both memristors and printed resistors make use of the crossbar structures for weighted-sum, their aging behavior is vastly different. To our knowledge, there is currently no design framework for printed neuromorphics that takes the aging of printed resistors into account.

3 METHODOLOGY

Figure 3 outlines our approach for aging-aware training for pNN under conductance variation. As the first step, we develop an aging model for the crossbar resistors. Then, based on the developed aging model, the aging-aware training objective and the gradient calculations required for gradient-based learning are described.

It should be noted that we do not consider the aging of the other printed hardware primitives, i.e., the activation and inverter circuits, in this work. To motivate this use case, one could assume that due to their uniformity, they could be manufactured in a high-volume production process such as roll-to-roll or screen printing together with passivation to prevent rapid aging. However, the crossbar conductances are customized afterward through low-cost inkjet-printing to achieve the desired functionality at the point of use. Hence, only the aging of the crossbar conductances is considered here.

3.1 Aging model for printed conductance

To study the aging of printed resistors, six printed (PEDOT [30]) resistors were fabricated, and their conductances were measured over 37 days. Five of them have different initial conductances, while two of them have the same initial conductance. Their conductance values over time are displayed in Figure 4.

We first process the measurement data by normalizing the time to an interval of $[0, 1]$. Furthermore, we divided the measured conductance values by the initial value $g_0 = g(0)$ to assess the relative conductance degradation. Similar to the aging behaviors of ITO resistors described in [27], all resistors display the aging behavior in the two regions: First, a relatively fast degradation followed by a more gradual phase (see Figure 5). Hence, we model a multiplicative

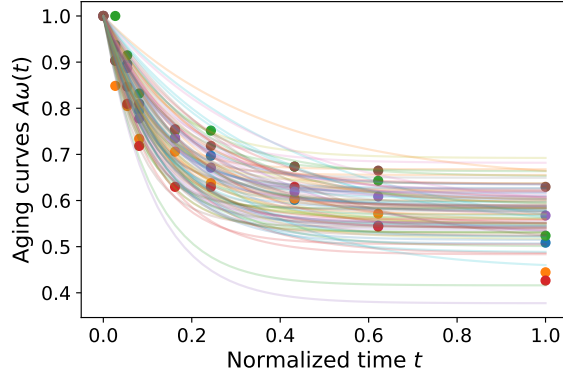


Figure 5: Curves from the aging model for sampled $\omega \sim p_\omega(\omega)$. The dots denote conductance measurements of printed resistors normalized by their initial conductance g_0 .

change of the initial conductance, i.e.,

$$g(t) = g_0 \cdot A_\omega(t), \quad (2)$$

and refer to the function $A_\omega(t)$ as the aging curve parameterized by the vector ω . Several functional forms can describe $A_\omega(t)$ such as a double linear model [51] or an exponential behavior which we will resort to in this work. We thus choose the following functional form

$$A_\omega(t) = \omega_1 \cdot e^{-\omega_2 \cdot t} - \omega_1 + 1,$$

with the fitting coefficients $\omega = [\omega_1, \omega_2]^\top$. Note that $A_\omega(0) = 1$, such that $g(0) = g_0$ at $t = 0$.

Since different resistors (even with the same initial conductance) display different aging behaviors over time, a variational model of the aging behaviors is required. For this purpose, we model the distributions of the fitting coefficients $p_\omega(\omega)$. To ensure a plausible functional form (i.e., monotonically decreasing) with respect to the observed behavior, ω_1 and ω_2 need to be positive. This can be achieved by modeling their distribution (either jointly or independently) using log-normal distributions. Note that also other distributions for positive random variables (e.g., the gamma distribution) could be used, depending on the quality of the fit.

After modeling the distributions of the fitting coefficients, we can generate multiple stochastic aging curves for a given conductance g_0 by sampling the fitted coefficients ω from the modeled distributions, i.e.,

$$g(t) = g_0 \cdot A_\omega(t) \quad \text{with } \omega \sim p_\omega(\omega) \quad (3)$$

Several aging curves $A_\omega(t)$ with sampled coefficients ω can be seen in Figure 5.

Finally, to assure that the aging curve $A_\omega(t)$ is independent of the initial conductance g_0 , we calculate the square of the correlation (r^2) between initial conductances and their corresponding coefficients ω_1, ω_2 for the six printed resistors. Their correlation coefficients are $r_{g_0, \omega_1}^2 = 0.04$ and $r_{g_0, \omega_2}^2 = 0.005$ respectively. Consequently, they are most likely (at least linear) independent of each other [42]. We thus conclude that the independence assumption is justified.

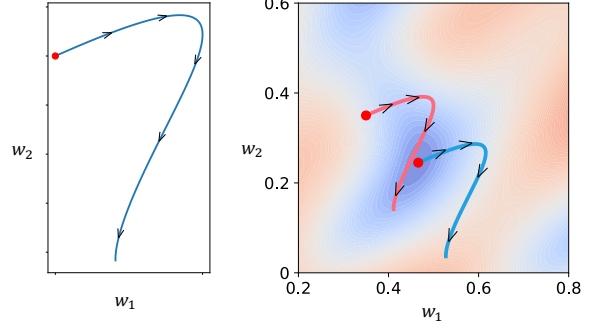


Figure 6: Exemplary aging trajectory of given weight $w(t)$ (left) and the optima of different objective functions (right). The red dots indicate the initial (non-aged) weights and the arrows represent the change in weights due to aging. The background contour in the right figure exemplifies a loss function $\mathcal{L}(\cdot)$, where red and blue denote regions of higher and lower loss respectively. The blue curve is the result of Equation 4, while the red curve is the result of Equation 5. Note that the shape of the aging trajectory may also depend on its starting location.

Discussion. In this work, we printed six resistors for building the mathematical aging model for printed resistors, and found a similar aging behavior to other works such as [27]. We described the aging behaviors $g(t)$ by the product of their initial conductances g_0 and the aging curves $A_\omega(t)$. Through more impeccable aging experiments and more data, the estimates of the distributions of the coefficients of the aging model could be improved. Furthermore, if deemed necessary, a better functional form $A_\omega(t)$ could be found to replace the function $A_\omega(t)$ developed above. However, as long as the function describing the aging behavior solely depends on the time t , no change to the aging-aware training described in the following section would be required.

3.2 Aging-aware training

In case of the nominal training of pNN (not considering aging), a loss function $\mathcal{L}\{\hat{y}(\theta, x), y\}$ is minimized to decrease the mismatch between the label y and the prediction of the pNN $\hat{y}(\theta, x)$ for an input x , i.e.,

$$\min_{\theta} \mathcal{L}\{\hat{y}(\theta, x), y\}. \quad (4)$$

However, as mentioned before, this formulation only optimizes for the (surrogate) conductance values immediately after fabrication, i.e., θ_0 . To account for the changes of the (surrogate) conductances over time, the whole trajectory of $\theta(t)$ over the lifetime has to be considered. This can be achieved by integrating the loss function over the lifetime, leading to the aging-aware training objective

$$\min_{\theta(t)} \int_{t=0}^1 \mathcal{L}\{\hat{y}(\theta(t), x), y\} dt.$$

We denote $\theta(t) = \theta_0 A_\omega(t)$ as the element-wise product of surrogate conductances θ_0 with their aging curves $A_\omega(t) = [A_{\omega_1}(t), A_{\omega_2}(t), \dots]^\top$, where $\omega_1, \omega_2, \dots$ are sampled values from $p_\omega(\omega)$.

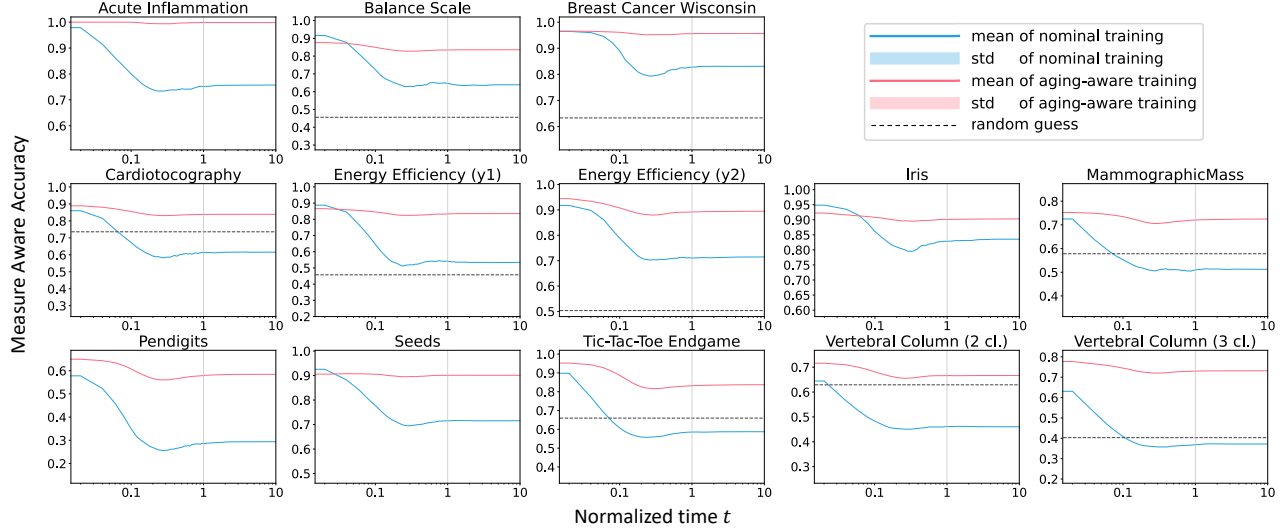


Figure 7: Measuring-aware accuracy of pNNs from nominal and aging-aware training on test set. The red lines and areas represent the accuracy and standard deviation of aging-aware training while the blues represent that of nominal training. The horizontal black dot lines indicate the result of random guess. Charts without black dot line mean that the accuracy of random guesses are lower than the range of charts. The gray vertical lines separate the extrapolation region from training region in terms of time.

Then, for fixed ω , the aging-aware training objective is given by

$$\min_{\theta_0} \int_{t=0}^1 \mathcal{L}\{\hat{y}(\theta_0 A_\omega(t), \mathbf{x}), \mathbf{y}\} dt. \quad (5)$$

Hence, (only) the starting point θ_0 of the aging path represents a learnable parameter. Figure 6 shows an exemplary aging trajectory of given weight $w(t)$ corresponding to the printed aging resistors in time t . We can see from the right side that, compared to the blue curve from Equation 4, the red curve from Equation 5 has a higher initial loss but lower average loss over the considered lifetime.

To additionally account the variations in the aging curves due to $p_\omega(\omega)$, we minimize for the expected loss with respect to $p_\omega(\omega)$, i.e.,

$$\min_{\theta_0} \mathbb{E}_{p_\omega(\omega)} \left\{ \int_{t=0}^1 \mathcal{L}\{\hat{y}(\theta_0 A_\omega(t), \mathbf{x}), \mathbf{y}\} dt \right\}. \quad (6)$$

In the following, we refer to "aging-aware training" when using this training objective.

Gradient-based learning. The use of gradient-based optimization for this objective requires the calculation of Equation 6. Unfortunately, the gradient cannot be calculated in closed form. Thus, an approximation is required. For this, we first reformulate the gradient of Equation 6 using the definition of the expected value and Leibniz rule [25]:

$$\begin{aligned} & \nabla_{\theta_0} \int_{\omega} \int_{t=0}^1 \mathcal{L}\{\hat{y}(\theta_0 A_\omega(t), \mathbf{x}), \mathbf{y}\} dt p_\omega(\omega) d\omega \\ &= \nabla_{\theta_0} \int_{\omega} \int_{t=0}^1 \mathcal{L}\{\hat{y}(\theta_0 A_\omega(t), \mathbf{x}), \mathbf{y}\} p_\omega(\omega) dt d\omega \\ &= \int_{\omega} \int_{t=0}^1 \nabla_{\theta_0} (\mathcal{L}\{\hat{y}(\theta_0 A_\omega(t), \mathbf{x}), \mathbf{y}\} p_\omega(\omega)) dt d\omega. \end{aligned}$$

Due to the independence of θ_0 and $p_\omega(\omega)$, we can further simplify the expression to

$$\begin{aligned} & \int_{\omega} \int_{t=0}^1 \nabla_{\theta_0} (\mathcal{L}\{\hat{y}(\theta_0 A_\omega(t), \mathbf{x}), \mathbf{y}\}) dt p_\omega(\omega) d\omega \\ &= \int_{\omega} \int_{t=0}^1 \nabla_{\theta_0} \mathcal{L}(\theta_0, \omega, t) dt p_\omega(\omega) d\omega \\ &= \mathbb{E}_{p_\omega(\omega)} \left\{ \int_{t=0}^1 \nabla_{\theta_0} \mathcal{L}(\theta_0, \omega, t) dt \right\} \end{aligned}$$

Based on this reformulation, we obtain an approximation to the expression using Monte-Carlo estimation. For this, we first express the integral over t as an expected value with respect to a uniform distribution $p_t(t) \sim \mathcal{U}[0, 1]$, i.e.,

$$\mathbb{E}_{p_\omega(\omega)} \left\{ \mathbb{E}_{p_t(t)} \left\{ \nabla_{\theta_0} \mathcal{L}(\theta_0, \omega, t) \right\} \right\}.$$

We then draw samples $\omega \sim p_\omega(\omega)$ and $t \sim p_t(t)$ resulting in gradient estimates

$$\frac{1}{N^\omega} \frac{1}{N^t} \sum_{\omega'} \sum_{t'} \nabla_{\theta_0} \mathcal{L}(\theta_0, \omega', t') \quad \text{with} \quad \begin{array}{l} t' \sim \mathcal{U}[0, 1], \\ \omega' \sim p_\omega(\omega), \end{array}$$

where N^ω is the number of samples ω' drawn from $p(\omega)$ and N^t is the number of samples t' drawn from $\mathcal{U}[0, 1]$ to approximate the integral over t .

This estimate can now be used for any gradient-based optimization algorithm such as Adam [34] in conjunction with the learning rules described in Section 2.2 to ensure the feasibility of the resulting conductance values. In addition, we can see that the derivation of the gradient estimate is independent of the specific choice of the functional form. Thus, one can easily adapt the functional form

Dataset	Topology	Classic accuracy		Measuring-aware accuracy		Baseline
		nominal	aging-aware	nominal	aging-aware	
Acute Inflammation [21]	6-3-2	0.857 ± 0.146	0.999 ± 0.006	0.757 ± 0.167	0.998 ± 0.012	0.417
Balance Scale [49]	4-3-3	0.832 ± 0.087	0.891 ± 0.031	0.641 ± 0.324	0.836 ± 0.038	0.456
Breast Cancer Wisconsin [40]	9-3-2	0.941 ± 0.088	0.966 ± 0.005	0.831 ± 0.204	0.956 ± 0.024	0.633
Cardiotocography [4]	21-3-3	0.832 ± 0.095	0.884 ± 0.019	0.616 ± 0.309	0.839 ± 0.037	0.736
Energy Efficiency [52] (y_1)	8-3-3	0.789 ± 0.154	0.871 ± 0.015	0.537 ± 0.285	0.835 ± 0.042	0.458
Energy Efficiency (y_2)	8-3-3	0.873 ± 0.072	0.925 ± 0.027	0.715 ± 0.157	0.894 ± 0.047	0.503
Iris [2]	4-3-3	0.927 ± 0.063	0.918 ± 0.022	0.834 ± 0.135	0.902 ± 0.033	0.300
Mammographic Mass [23]	5-3-2	0.618 ± 0.146	0.767 ± 0.012	0.514 ± 0.151	0.724 ± 0.042	0.578
Pendigits [1]	16-3-10	0.563 ± 0.112	0.746 ± 0.024	0.294 ± 0.131	0.583 ± 0.057	0.099
Seeds [14]	7-3-3	0.845 ± 0.116	0.936 ± 0.020	0.717 ± 0.168	0.901 ± 0.036	0.333
Tic-Tac-Toe Endgame [41]	9-3-2	0.671 ± 0.226	0.875 ± 0.086	0.588 ± 0.214	0.837 ± 0.106	0.660
Vertebral Column [5] (2 cl.)	6-3-2	0.628 ± 0.109	0.737 ± 0.032	0.462 ± 0.181	0.667 ± 0.053	0.629
Vertebral Column (3 cl.)	6-3-3	0.586 ± 0.144	0.778 ± 0.030	0.373 ± 0.151	0.731 ± 0.047	0.403
Average	-	0.766 ± 0.120	0.869 ± 0.025	0.606 ± 0.198	0.823 ± 0.044	0.477

Table 1: The mean and standard deviation of the average (over time) ACC/MAA of nominal training and aging-aware training. The baseline refers to always selecting the most frequent class in the combined training and validation set.

$A_\omega(t)$ without changing the aging-aware training, as long as $A_\omega(t)$ does not depend on the initial conductance θ_0 .

4 EXPERIMENTS

To evaluate the effectiveness of the aging-aware training, we implemented the proposed training approach¹ in PyTorch [44], and compared the algorithm with nominal training using Equation 4 on the 13 benchmark datasets, whose complexities and use cases match the PE profile appropriately and were also used in [55]. Consequently, we also use the preprocessed datasets from [24]. Finally, as in [57], the inputs are normalized to $[0, 1]$ to simulate the electrical signals from sensors.

4.1 Experiment Setup

We first split the datasets into training (60%), validation (20%), and test (20%) sets with a fixed random seed. Then we repeated both nominal and aging-aware training over ten (identical for both methods) random seeds.

Hyperparameter. We set a fixed $m = 0.3$ as training margin for the loss function and a measuring threshold of $T = 0.1$ (details about hardware-related hyperparameters, see [56]). Additionally, we use the same topology #inputs-3-#outputs for all pNNs as described in [55]. In terms of training-related hyperparameters, we set the learning rates for both nominal and aging-aware training to 0.1. In addition, we selected $N_{\text{train}}^\omega = 50$ and $N_{\text{train}}^T = 10$ samples for Monte-Carlo integration during aging-aware training, and $N_{\text{valid}}^\omega = 20$, $N_{\text{valid}}^T = 10$ during validation.

Training & Validation. We use full batches for gradient calculation and Adam [34] with default parameters for both nominal and aging-aware training for parameter updates. After each training epoch, we calculated the loss on the validation set.

In nominal training, we performed early-stopping after training at least 20 000 epochs to ensure that the parameters are trained to

an optimum on each dataset. We then choose the parameters of pNN with the minimum loss on the validation set as the final result.

In aging-aware training, the parameters are trained in 800 epochs without early-stopping. Analogous to nominal training, we also calculated the loss on the validation set after each training epoch. Although there is an apparent decreasing tendency of the loss on the validation set during training, the loss on the validation set fluctuates drastically due to the Monte-Carlo sampling. Therefore, the early-stop strategy is not suitable for aging-aware training. Nevertheless, we still choose the parameters with the lowest loss on the validation set as the final result.

Baseline. As the baseline, we report the performance of *random guess*, i.e., to always predict the most frequent class from the combined training and validation set. Hence, if the pNN gets worse than this baseline, there is no benefit to considering the output of the pNN anymore.

4.2 Result

After training, we choose pNNs based on the best validation loss, as it would be the one selected for fabrication. We evaluate the results of the test set. The pNNs are not only evaluated within the normalized time interval $[0, 1]$ (training interval of 37 days), but also extended to $[0, 10]$, which represents an extrapolation to approximately one year. As an evaluation metric, we select the classic accuracy (ACC) and measuring-aware accuracy (MAA) [56], where ACC represents the accuracy in a general sense and MAA is hardware-related accuracy, considering the threshold for measuring voltages, etc. We report the mean and standard deviation of both metrics base on $N_{\text{test}}^\omega = 500$ sampled aging curves. Generally, aging-aware training leads to better results, see Figure 7. Moreover, since the conductance decay exponentially over time, only slight changes in the conductances in the interval $[1, 10]$ can be observed. Thus, the accuracy is stable in this region. To measure the results of each dataset in a single metric, we average the mean ACC/MAA over time, see Table 1. From this table, we can conclude that, compared to nominal training, aging-aware training has a higher expectation of

¹The code is currently available at <https://github.com/Neuromorphic/Aging-aware-training>

accuracy throughout the lifetime, and it is more robust against the expected aging behaviors based on our aging model. To summarize the overall improvement, we average the accuracy cross all datasets and calculate the improvement of averaged aging-aware training (relative to nominal training) across all datasets. The result reflects an overall 35.8% improvement in the expected accuracy of aging-aware training over nominal training.

4.3 Discussion

In contrast to nominal training, which aims to achieve the best accuracy at t_0 , aging-aware training focuses on improving the expected accuracy over the circuit lifetime by considering the aging of the printed crossbar resistors. Therefore, with the same number of learnable parameters, the nominal training may outperform aging-aware training at t_0 , while over a longer time horizon, pNNs from aging-aware training may display a better accuracy. Moreover, since the aging-aware training considers the variation of stochastic aging curves, pNNs from aging-aware training should display more stable results (i.e. less standard deviation) when subjected to aging. This is also what can be observed in Figure 7.

However, for some datasets, the results of aging-aware training even exceed those of nominal training at t_0 , see *Cardiotocography*, *Energy Efficiency* (y_2), *Pendigits*, and *Vertebral Column*. This is possibly due to favorable optimization dynamics through sampling. For example, since aging-aware training samples and calculates gradients for several sets of parameters in the vicinity of the current solution, it may have an easier time escaping local minima.

It should be mentioned that, as a trade-off for high expected accuracy, aging-aware training requires a longer runtime due to sampling and additional gradient computations. Since the gradient computation is the most costly operations, the training time for aging-aware training is approximately $N^\omega \times N^t$ times that of nominal training (if no parallelism is employed).

5 CONCLUSION AND FUTURE WORK

Due to its advantages such as ultra-low costs and flexibility, printed electronics has been taking over several emerging fields like IoT and wearable technologies. With the incorporation of the artificial neural networks which achieve high efficiency with extremely simple primitives, printed neuromorphic computing becomes even more of a marvel. However, the aging of printed components is a decisive problem that cannot be ignored.

In this work, we proposed an aging-aware training framework for pNN to address the aging problem of printed components in printed neuromorphic circuits. For this purpose, we developed a stochastic aging model for the printed resistors. We then formulated an objective function that encourages a pNN, based on an aging model, to achieve higher expected accuracy over a device lifetime. Since no closed expression for the gradients of the training objective can be derived, gradients were estimated using Monte-Carlo (gradient) estimation.

Our experiments show that training pNNs through the proposed aging-aware training framework can substantially improve the expected accuracy under the modeled aging behavior. This should, in turn, lead to the printed neuromorphic circuits exhibiting a better overall accuracy over their lifetime.

As a limitation, only the aging of the crossbar resistors, which represent the weights, was considered. The other circuit components, i.e., activation and negative-weight circuits, were assumed to exhibit no aging due to the prefabrication and passivation. However, aging in these components should also be considered for future work. Additionally, the initial conductance value was assumed to be fabricated precisely. However, due to the variations associated with PE, manufacturing variations in the initial conductance value should also be considered in the future.

ACKNOWLEDGMENTS

This work was partially founded by the KIT Centers pilot project SoftNeuRo and the Ministry of Science, Research and Arts of the state of Baden-Württemberg in form of the MERAGEM doctoral program.

REFERENCES

- [1] Fevzi Alimoglu, Dr Doc, Ethem Alpaydin, and Yagmur Denizhan. 1996. Combining Multiple Classifiers for Pen-based Handwritten Digit Recognition. (1996).
- [2] Edgar Anderson. 1935. The Irises of The Gaspe Peninsula. *Bull. Am. Iris Soc.* 59 (1935), 2–5.
- [3] CL Au, WA Anderson, DA Schmitz, JC Flassayer, and FM Collins. 1990. Stability of Tantalum Nitride Thin Film Resistors. *Journal of Materials Research* 5, 6 (1990), 1224–1232.
- [4] Diogo Ayres-de Campos, Joao Bernardes, Antonio Garrido, Joaquim Marques-de Sa, and Luis Pereira-Leite. 2000. Sisporto 2.0: A Program for Automated Analysis of Cardiotocograms. *Journal of Maternal-Fetal Medicine* 9, 5 (2000), 311–318.
- [5] Eric Berthonnaud, Joannès Dimnet, Pierre Roussouly, and Hubert Labelle. 2005. Analysis of The Sagittal Balance of The Spine and Pelvis Using Shape and Orientation Parameters. *Clinical Spine Surgery* 18, 1 (2005), 40–47.
- [6] U Bielecka, P Lutsyk, K Janus, J Sworakowski, and W Bartkowiak. 2011. Effect of solution aging on morphology and electrical characteristics of regioregular P3HT FETs fabricated by spin coating and spray coating. *Organic Electronics* 12, 11 (2011), 1768–1776.
- [7] Detlef Bonfert, Dieter Hemmetzberger, Gerhard Klink, and Karlheinz Bock. 2012. Ageing Behavior of Printed Flexible Resistors By Thermal, Mechanical and Electrical Stresses. In *2012 4th Electronic System-Integration Technology Conference*. IEEE, 1–6.
- [8] Jason J Braithwaite, Derrick G Watson, Robert Jones, and Mickey Rowe. 2013. A Guide for Analysing Electrodermal Activity (EDA) & Skin Conductance Responses (SCRs) for Psychological Experiments. *Psychophysiology* 49, 1 (2013), 1017–1034.
- [9] G Bulger. 1975. Stability Analysis of Laser Trimmed Thin Film Resistors. *IEEE Transactions on Parts, Hybrids, and Packaging* 11, 3 (1975), 172–177.
- [10] Gabriel Cadilha Marques, Dennis Weller, Ahmet Turan Erozan, Xiaowei Feng, Mehdi Tahoori, and Jasmin Aghassi-Hagmann. 2019. Progress Report on "From Printed Electrolyte-Gated Metal-Oxide Devices to Circuits". *Advanced Materials* (2019), 1806483.
- [11] SP Carfagno and RJ Gibson. 1980. *A Review of Equipment Aging Theory and Technology*. Electric Power Research Institute.
- [12] Joseph S Chang, Antonio F Facchetti, and Robert Reuss. 2017. A Circuits and Systems Perspective of Organic/printed Electronics: Review, Challenges, and Contemporary and Emerging Design Approaches. *IEEE Journal on emerging and selected topics in circuits and systems* 7, 1 (2017), 7–26.
- [13] J. S. Chang, A. F. Facchetti, and R. Reuss. 2017. A Circuits and Systems Perspective of Organic/printed Electronics: Review, Challenges, and Contemporary and Emerging Design Approaches. *IEEE Journal on Emerging and Selected Topics in Circuits and Systems* 7, 1 (2017), 7–26.
- [14] Małgorzata Charytanowicz, Jerzy Niewczas, Piotr Kulczycki, Piotr A Kowalski, Szymon Łukasik, and Sławomir Żak. 2010. Complete Gradient Clustering Algorithm for Features Analysis of X-ray Images. In *Information technologies in biomedicine*. Springer, 15–24.
- [15] Peng-Yu Chen, Chih-Lei Chen, Chien-Chuan Chen, Lun Tsai, Hung-Che Ting, Li-Fong Lin, Chih-Cheng Chen, Chia-Yu Chen, Lee-Hsun Chang, Tsung-Hsiang Shih, et al. 2014. 30.1: Invited Paper: 65-Inch Inkjet Printed Organic Light-Emitting Display Panel with High Degree of Pixel Uniformity. In *SID Symposium Digest of Technical Papers*, Vol. 45. Wiley Online Library, 396–398.
- [16] Seungjun Chung, Seul Ong Kim, Soon-Ki Kwon, Changhee Lee, and Yongtaek Hong. 2011. All-inkjet-printed Organic Thin-film Transistor Inverter on Flexible Plastic Substrate. *IEEE electron device letters* 32, 8 (2011), 1134–1136.

- [17] W. Clemens, W. Fix, J. Ficker, A. Knobloch, and A. Ullmann. 2004. From Polymer Transistors Toward Printed Electronics. *Journal of Materials Research* 19, 7 (July 2004), 1963–1973. <https://doi.org/10.1557/jmr.2004.0263>
- [18] M Coleman. 1984. Ageing Mechanisms and Stability in Thick Film Resistors. *Microelectronics International* (1984).
- [19] Silvia Conti, Lorenzo Pimpolari, Gabriele Calabrese, Robyn Worsley, Subimal Majee, Dmitry K Polyushkin, Matthias Paur, Simona Pace, Dong Hoon Keum, Filippo Fabbri, et al. 2020. Low-voltage 2d Materials-based Printed Field-effect Transistors for Integrated Digital and Analog Electronics on Paper. *Nature communications* 11, 1 (2020), 1–9.
- [20] Zheng Cui. 2016. *Printed Electronics: Materials, Technologies and Applications*. John Wiley & Sons.
- [21] Jacek Czerniak and Hubert Zarzycki. 2003. Application of Rough Sets in The Presumptive Diagnosis of Urinary System Diseases. In *Artificial intelligence and security in computing systems*. Springer, 41–51.
- [22] Alejandro de la Fuente Vornbrock, Donovan Sung, Hongki Kang, Rungrot Kit-somboonloha, and Vivek Subramanian. 2010. Fully gravure and ink-jet printed high speed pBTTT organic thin film transistors. *Organic Electronics* 11, 12 (2010), 2037–2044.
- [23] Matthias Elter, Rüdiger Schulz-Wendtland, and Thomas Wittenberg. 2007. The Prediction of Breast Cancer Biopsy Outcomes Using Two Cad Approaches That Both Emphasize an Intelligible Decision Process. *Medical physics* 34, 11 (2007), 4164–4172.
- [24] Manuel Fernández-Delgado, Eva Cernadas, Senén Barro, and Dinani Amorim. 2014. Do We Need Hundreds of Classifiers To Solve Real World Classification Problems? *The journal of machine learning research* 15, 1 (2014), 3133–3181.
- [25] Harley Flanders. 1973. Differentiation Under The Integral Sign. *The American Mathematical Monthly* 80, 6 (1973), 615–627.
- [26] B Fraboni, Piero Cosseddu, YQ Wang, RK Schulze, ZF Di, A Cavallini, M Nastasi, and A Bonfiglio. 2011. Aging control of organic thin film transistors via ion-implantation. *Organic Electronics* 12, 9 (2011), 1552–1559.
- [27] Mohammad M Hamasha, Tara Dhakal, Khalid Alzoubi, Shehab Albahri, Awni Qasameh, Susan Lu, and Charles R Westgate. 2012. Stability of ITO thin film on flexible substrate under thermal aging and thermal cycling conditions. *Journal of Display Technology* 8, 7 (2012), 385–390.
- [28] B Huber, PB Popp, M Kaiser, A Ruediger, and C Schindler. 2017. Fully Inkjet Printed Flexible Resistive Memory. *Applied Physics Letters* 110, 14 (2017), 143503.
- [29] Woo Jin Hyun, Ethan B Secor, Mark C Hersam, C Daniel Frisbie, and Lorraine F Francis. 2015. High-resolution patterning of graphene by screen printing with a silicon stencil for highly flexible printed electronics. *Advanced Materials* 27, 1 (2015), 109–115.
- [30] C Ionescu, P Svasta, A Vasile, and D Bonfert. 2012. Investigations on organic printed resistors based on PEDOT: PSS. In *2012 IEEE 18th International Symposium for Design and Technology in Electronic Packaging (SIITME)*. IEEE, 85–89.
- [31] Aidana Imranova, Akshay Maan, Alex James, and Leon Chua. 2020. Analog Self-timed Programming Circuits for Aging Memristors. *IEEE Transactions on Circuits and Systems II: Express Briefs* 68, 4 (2020), 1133–1137.
- [32] Saleem Khan, Leandro Lorenzelli, and Ravinder S Dahiya. 2014. Technologies for Printing Sensors and Electronics over Large Flexible Substrates: A Review. *IEEE Sensors Journal* 15, 6 (2014), 3164–3185.
- [33] Sangkil Kim, Manos M Tentzeris, and Apostolos Georgiadis. 2019. Hybrid Printed Energy Harvesting Technology for Self-Sustainable Autonomous Sensor Application. *Sensors* 19, 3 (2019), 728.
- [34] Diederik P Kingma and Jimmy Ba. 2014. Adam: A Method for Stochastic Optimization. *arXiv preprint arXiv:1412.6980* (2014).
- [35] G Kirchhoff. 1850. LXIV. On a Deduction of Ohm's Laws, in connexion with the Theory of Electro-statics. *The London, Edinburgh, and Dublin Philosophical Magazine and Journal of Science* 37, 252 (1850), 463–468.
- [36] Masaya Kondo, Takafumi Uemura, Mihoko Akiyama, Naoko Namba, Masahiro Sugiyama, Yuki Noda, Teppei Araki, Shusuke Yoshimoto, and Tsuyoshi Sekitani. 2018. Design of Ultraflexible Organic Differential Amplifier Circuits for Wearable Sensor Technologies. In *2018 IEEE International Conference on Microelectronic Test Structures (ICMTS)*. IEEE, 79–84.
- [37] Jongwoo Lim, Hyunsung Jung, Changyeon Baek, Geon-Tae Hwang, Jungho Ryu, Daeho Yoon, Jiboom Yoo, Kwi-il Park, and Jong Hee Kim. 2017. All-inkjet-printed flexible piezoelectric generator made of solvent evaporation assisted BaTiO₃ hybrid material. *Nano Energy* 41 (2017), 337–343.
- [38] Kuankuan Lu, Rihui Yao, Yiping Wang, Honglong Ning, Dong Guo, Xianzhe Liu, Ruiqiang Tao, Miao Xu, Lei Wang, and Junbiao Peng. 2019. Effects of praseodymium doping on the electrical properties and aging effect of InZnO thin-film transistor. *Journal of Materials Science* 54, 24 (2019), 14778–14786.
- [39] Travis C Mallett. 2019. Aging in Commercial Thick-and Thin-Film Resistors: Survey and Uncertainty Analysis. *IEEE Transactions on Instrumentation and Measurement* 68, 11 (2019), 4190–4204.
- [40] Olvi L Mangasarian and William H Wolberg. 1990. *Cancer Diagnosis Via Linear Programming*. Technical Report. University of Wisconsin-Madison Department of Computer Sciences.
- [41] Christopher J Matheus and Larry A Rendell. 1989. Constructive Induction on Decision Trees.. In *IJCAI*, Vol. 89. Citeseer, 645–650.
- [42] David S Moore, William I Notz, and William Notz. 2006. *Statistics: Concepts and Controversies*. Macmillan.
- [43] Muhammad Husnain Mubarik, Dennis D Weller, Nathaniel Bleier, Matthew Tomei, Jasmin Aghassi-Hagmann, Mehdi B Tahoori, and Rakesh Kumar. 2020. Printed Machine Learning Classifiers. In *2020 53rd Annual IEEE/ACM International Symposium on Microarchitecture (MICRO)*. IEEE, 73–87.
- [44] Adam Paszke, Sam Gross, Francisco Massa, Adam Lerer, James Bradbury, Gregory Chanan, Trevor Killeen, Zeming Lin, Natalia Gimelshein, Luca Antiga, Alban Desmaison, Andreas Kopf, Edward Yang, Zachary DeVito, Martin Raison, Alykhan Tejani, Sasank Chilamkurthy, Benoit Steiner, Lu Fang, Junjie Bai, and Soumith Chintala. 2019. Pytorch: an Imperative Style, High-performance Deep Learning Library. In *Advances in Neural Information Processing Systems* 32. H. Wallach, H. Larochelle, A. Beygelzimer, F. d'Alché-Buc, E. Fox, and R. Garnett (Eds.). Curran Associates, Inc., 8024–8035.
- [45] Jolke Perelaer, Patrick J. Smith, Dario Mager, Daniel Soltman, Steven K. Volkman, Vivek Subramanian, Jan G. Korvink, and Ulrich S. Schubert. 2010. Printed Electronics: The Challenges Involved in Printing Devices, Interconnects, and Contacts Based on Inorganic Materials. *Journal of Materials Chemistry* 20, 39 (2010), 8446. <https://doi.org/10.1039/c0jm00264j>
- [46] Farhan Rasheed, Michael Hefenbrock, Michael Beigl, Mehdi B Tahoori, and Jasmin Aghassi-Hagmann. 2018. Variability Modeling for Printed Inorganic Electrolyte-Gated Transistors and Circuits. *IEEE transactions on electron devices* 66, 1 (2018), 146–152.
- [47] Paulo Rosa, António Câmara, and Cristina Gouveia. 2015. The Potential of Printed Electronics and Personal Fabrication in Driving the Internet of Things. *Open Journal of Internet Of Things (OJIoT)* 1, 1 (2015), 16–36.
- [48] Feng Sha and Qing Wan. 2019. Recent Progress on Jet Printing of Oxide-based Thin Film Transistors. *Journal of Physics D: Applied Physics* 52, 14 (2019), 143002.
- [49] Robert S Siegler. 1976. Three Aspects of Cognitive Development. *Cognitive psychology* 8, 4 (1976), 481–520.
- [50] FN Sinnadurai, PE Spencer, and KJ Wilson. 1980. Some Observations on The Accelerated Ageing of Thick-film Resistors. *Electrocomponent Science and Technology* 6, 3–4 (1980), 241–246.
- [51] NIHAL Sinnadurai and K Wilson. 1982. The Aging Behavior of Commercial Thick-film Resistors. *IEEE Transactions on Components, Hybrids, and Manufacturing Technology* 5, 3 (1982), 308–317.
- [52] Athanasios Tsanas and Angeliki Xifara. 2012. Accurate Quantitative Estimation of Energy Performance of Residential Buildings Using Statistical Machine Learning Tools. *Energy and Buildings* 49 (2012), 560–567.
- [53] Fabrizio A Viola, Biagio Brigitte, Paolo Colpani, Giorgio Dell'Erba, Virgilio Mattoli, Dario Natali, and Mario Caironi. 2020. A 13.56 MHz Rectifier Based on Fully Inkjet Printed Organic Diodes. *Advanced Materials* (2020), 2002329.
- [54] Dennis Weller, Gabriel Cadilha Marques, Jasmin Aghassi-Hagmann, and Mehdi B Tahoori. 2018. An Inkjet-printed Low-voltage Latch Based on Inorganic Electrolyte-gated Transistors. *IEEE Electron Device Letters* 39, 6 (2018), 831–834.
- [55] Dennis D Weller, Nathaniel Bleier, Michael Hefenbrock, Jasmin Aghassi-Hagmann, Michael Beigl, Rakesh Kumar, and Mehdi B Tahoori. 2021. Printed Stochastic Computing Neural Networks. In *2021 Design, Automation & Test in Europe Conference & Exhibition (DATE)*. IEEE, 914–919.
- [56] Dennis D Weller, Michael Hefenbrock, Michael Beigl, Jasmin Aghassi-Hagmann, and Mehdi B Tahoori. 2021. Realization and Training of an Inverter-based Printed Neuromorphic Computing System. *Scientific reports* 11, 1 (2021), 1–13.
- [57] Dennis D Weller, Michael Hefenbrock, Mehdi B Tahoori, Jasmin Aghassi-Hagmann, and Michael Beigl. 2020. Programmable Neuromorphic Circuit Based on Printed Electrolyte-Gated Transistors. In *2020 25th Asia and South Pacific Design Automation Conference (ASP-DAC)*. IEEE, 446–451.
- [58] Penghang Yin, Jiancheng Lyu, Shuai Zhang, Stanley Osher, Yingyong Qi, and Jack Xin. 2019. Understanding Straight-Through Estimator in Training Activation Quantized Neural Nets. *arXiv preprint arXiv:1903.05662* (2019).
- [59] Haibin Zhao, Tobias Röddiger, and Michael Beigl. 2021. Aircase: Earable Charging Case With Air Quality Monitoring and Soundscape Sonification. In *Adjunct Proceedings of the 2021 ACM International Joint Conference on Pervasive and Ubiquitous Computing and Proceedings of the 2021 ACM International Symposium on Wearable Computers*. 180–184.